LEWIS NAYLOR

An Investigation into Gallium Lanthanum Sulfide as a Solid-state Electrolyte

FINAL YEAR BSC

PROJECT REPORT 2023/2024

This report is presented in partial fulfilment of the requirements for the award of the degree of B.Sc. with Honours in Physics

Abstract:

Devices using gallium lanthanum sulfide (GaLaS) as a solid-state electrolyte (SSE) were fabricated, with ITO and Al electrodes, via thin-film evaporation. Differing amounts of Li_2S were co-evaporated with the GaLaS and their electrical properties were investigated via voltage sweeps and impedance sweeps, from a control result of 10^{-13} S cm^{-1} the highest conductivity observed in this investigation was of 10^{-6} S cm^{-1} and based upon bandgap calculations and electrochemical impedance analysis it is assumed that the conduction mechanism was via ionic conduction, showing great potential for GaLaS as an SSE as this conductivity was achieved at relatively low concentrations of Li. It was observed that the devices are only roughly Ohmic at ≤ 1V ranges while at higher voltages the appearance of the Al electrode changed, believed to be alloying between the Al and the Li being the likely cause of the electrical properties becoming non-Ohmic.

Acknowledgement:

I would like to give thanks to Dr Mark Hughes for his support, critique and expert guidance throughout the entirety of this investigation.

Contents

1. Introduction 5
2. Methodology 6
   2.1 Fabrication of Devices 6
   2.2 Testing of Devices 9
3. Results and Discussion 10
   3.1 Control (BGW1) 10
   3.2 LN1 12
   3.3 LN2 16
   3.4 LN3 21
   3.5 Absorption Spectra 27
   3.6 Final Results 29
4. Conclusion 30
5. Bibliography 30

1. Introduction

With the increase of battery dependent devices for use in daily life it is necessary that batteries these devices are dependent on keep advancing in their safety, durability, and capacity and with the increasing effects of climate change it is paramount that more renewable energy is used with this energy needing to be stored [1]. Inorganic solid-state electrolytes are an ideal solution for these problems due to their shown improvements on reliability and safety compared to organic-based liquid electrolyte batteries [2]. Sulfide-based glasses have been shown to be good candidates for use as solid-state electrolytes (SSE) due to their high conductivity of lithium ions shown in Q. Zang et al.'s comprehensive review of a broad range of sulfide-based glasses, table 1.1 shows the conductivities of a range of sulfide-based chalcogenides glasses covered within the review.

Material	Conductivity (S cm^{-1})
$Li_{10}GeP_2S_{12}$	1.2×10^{-2}
$80Li_2S{\cdot}20P_2S_5$	1.3×10^{-4}
$70Li_2S{\cdot}30P_2S_5$	3.7×10^{-5}
$60Li_2S{\cdot}40P_2S_5$	3.2×10^{-6}
$Li_7P_3S_{11}$	3.2×10^{-3}

Table 1.1: Ionic conductivity of sulfide-based solid electrolytes. Data reproduced from [3].

$Li_{10}GeP_2S_{12}$ demonstrated by N Kayama et al. represents one of the highest conductivities recorded for an SSE at room temperature of 1.2×10^{-2} S cm^{-1} with its high lithium-ion conductivity due to its crystal structure allowing excellent ionic conduction through the sample [4].

Gallium lanthanum sulfide (GaLaS) has been identified as a good candidate for usage as an SSE due to its lack of toxic materials once it is refined compared to other arsenic-based chalcogenide glasses, its durability, and its thermal stability. GaLaS's Young's modulus of 59 GPa [5] is exceptionally high compared to other chalcogenide glasses, see table 1.2, which is a huge benefit for its potential use cases within devices such as mobile phones and electric vehicles where forces are likely to be imparted on the device.

Material	Young's Modulus (GPa)	References
GaLaS	59	[5]
GeSe	11	[5]
A1	18.14	[6]
A2	20.35	[6]
A3	21.84	[6]
A4	20.24	[6]
A5	18.53	[6]

Table 1.2: Young's modulus for select chalcogenide glasses. See table 1.3 for the chemical compositions of materials A1-5.

Material	Ge (%)	Sb (%)	Se (%)
A1	13.3	13.3	73.4
A2	18.2	18.2	63.6
A3	20	20	60
A4	23.3	13.3	63.7
A5	25	10	65

Table 1.3: Chemical compositions of chalcogenide glasses referred to in table 1.2. Data reproduced from [6].

GaLaS's glass transition temperature (T_g) of 559 °C [5] is much greater than that of other chalcogenides, see table 1.4 [7][8], which is desirable as it presents a wider potential operational range for GaLaS based devices.

Chalcogenide	T_g (°C)
GaLaS	559
GeS	456
GeSe	324
As_2S_3	200
$Ge_{20}Te_{80}$	159
$Ge_2Sb_2Te_5$	100

Table 1.4: Thermal properties of select chalcogenide solid-state electrolytes. Data reproduced from [5].

2. Methodology

2.1 Fabrication of Devices

Devices for this investigation were produced via thin film deposition. Initial slides of silicon oxide (SiO_2) with a layer of indium tin oxide (ITO) deposited onto only one surface to provide a conductive medium were first acquired. These substrates were loaded onto the stage of the device with the vacuum chamber lowered to a maximum pressure of 1×10^{-5} mBar. During deposition the stage was rotated at 5 rpm to ensure full coverage across the surface of the device.

For the control device (BGW1) a sample of GaLaS was then crushed into a powder then loaded into a crucible of the deposition device. This crucible was then heated via an electron beam with the power being varied during evaporation to have a deposition rate between 1 and 2 Å s^{-1} measured via the quartz crystal monitor (QCM).

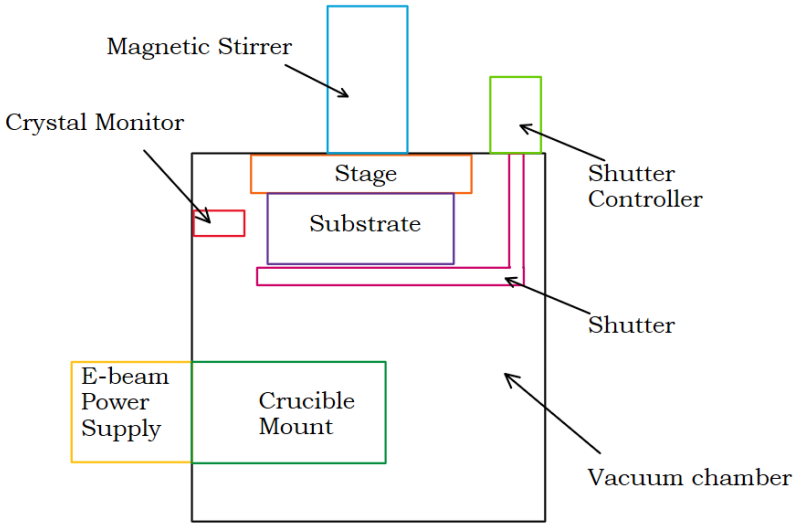

Figure 2.1.1: Schematic diagram of the Korvus Hex Thin Film Deposition device used to fabricate the devices.

For the testing devices the GaLaS is co-evaporated with Li_2S in a separate crucible, based upon the evaporation for GaLaS for the control device, the GaLaS power was set to 45W while the power to the Li_2S crucible was set to different levels of power for each device fabricated therefore, each device had differing quantities of Li_2S. The knowledge of the different powers coupled with the rate of deposition recorded by the QCM allowed an estimate for the ratio between the GaLaS and Li_2S in the conduction layer to be formed. This is given as a rough estimate as the QCM can only give the rate based on a single density of a material. At the start of the evaporation only the Li_2S layer is heated with the density of Li_2S, 1.66 g cm^{-3} used in determining the deposition rate. The power the Li_2S crucible for this device is then set based on the rate of deposition desired and held constant, the value of density for the QCM is then set back to the density of GaLaS, 4.04gcm^{-3}, and the GaLaS crucible is then heated with the rate of deposition aimed to be between 1 and 2 Ås^{-1} as the density of GaLaS is 2.4 times that of Li_2S it is assumed that the rate recorded is entirely that of GaLaS while assuming the value of Li_2S deposition rate staying constant for the entire course of the fabrication. Figure 2.1.3 shows data for the co-evaporation of GaLaS and Li_2S for device LN3 (note the initial power for the Li_2S was to evaporate off any lithium hydroxide that may have formed before the evaporation). The total thickness of this layer, hence called the "conduction layer", is no thinner than 1000 Å for all devices.

After completion of the conduction layer deposition a mask containing a grid of 1mm^2 holes was placed over the device with aluminium (Al) strips added to a separate crucible of the device. This crucible was then heated to deposit a grid of Al onto the devices to create contact pads for usage in testing.

During this investigation a total of four devices were fabricated, their names and associated powers supplied to the crucibles during fabrication are shown in table 2.1.2.

Device	Average GaLaS Power (W)	Average Li_2S Power (W)
BGW1 (Control)	~45	0
LN1	~50	~10
LN2	51.5144	52.5266
LN3	62.2473	32.0106

Table 2.1.2: Devices fabricated in this investigation and their associated powers.

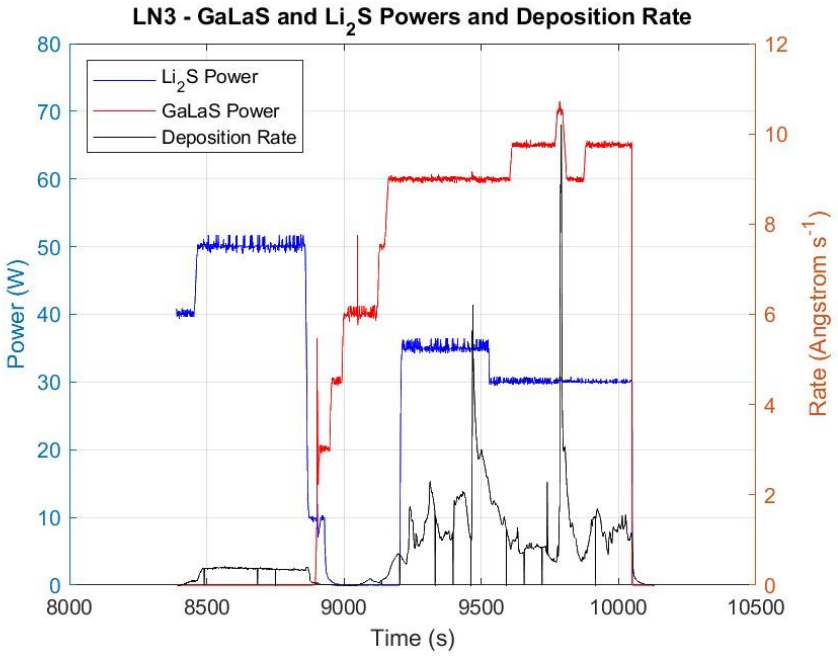

Figure 2.1.3: Plot of rate vs time and pover vs time for the evaporation of GaLaS and Li2S for device LN3.

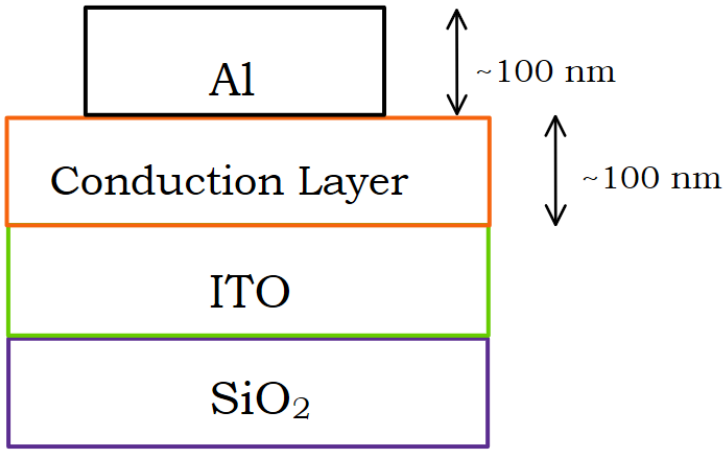

Figure 2.1.4: Cross-sectional schematic diagram of device.

2.2 Testing of Devices

The properties of devices created were examined via three main methods, via recording the current through the device at varying voltages, an I-V sweep and via measuring the impedance and recording of absorption spectra. For recording of results each pad on each device was named, devices were marked in on corner of the device with the horizontal axis indexed alphabetically and the vertical axis indexed numerically.

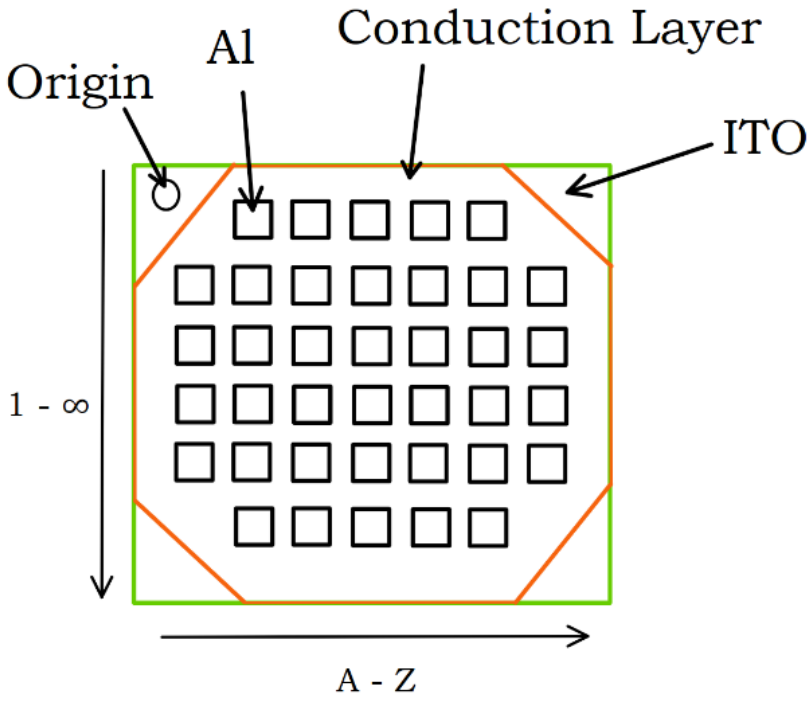

Figure 2.2.1: Top-view schematic diagram of device with indexing axes.

For the I-V sweeps two wire probes are placed in contact with the device, one contacting the ITO layer and another in contact with one of the aluminium pads of the device. These probes are connected to a source measure unit, the ITO probe connected to “Output Low” and the Al pad probe connected to “Output High”, this setup is so the voltage across the device is from the pad to the ITO when set within the control software.

To ensure the safety of the device a maximum current through circuit was set to be 10mA. The voltage across the device would then be varied with the current through the device recorded, from these values the resistance and resistivity can be found, these results compared to the control shows the effect that the Li_2S has on the device. Results were taken as “sweeps up” where the voltage is swept from a negative voltage to a positive voltage, “sweeps down” where the voltage is swept from a positive to negative and cyclic where the voltage is swept from positive to negative then back to positive.

To test the impedance the device, again two wire probes are used, one contacted to the ITO and the other contacting one of the Al pads. In this testing the voltage of the oscillation is set, in this

investigation no larger than 1V, and then a range of frequencies is set, with the maximum range being 5Hz – 13MHz. The results from these sweeps can be used to determine the nature of conduction in the conduction layer, for this investigation the nature of conduction desired is via lithium ions.

Absorption spectra were taken via usage of a Cary 60 UV-Vis Spectrophotometer in a wavelength range of 1100nm and 190nm, from this data the concentration of Li_2S can be found for each device.

3. Results and Discussion

In the scope of this investigation four devices were fabricated. One control device consisting of a conduction layer entirely of GaLaS and three test devices with varying levels of Li_2S within the conduction layer.

To analyse the results from each device the resistivity must first be calculated using:

$$\rho = \frac{RA}{l}, \tag{1}$$

where ρ is the resistivity in Ω cm, R is the resistance in Ω, A is the cross-sectional area in cm^2 and l is the length of the device in cm. Taking l to be the depth of the conduction layer, 1×10^{-5}cm and A to be the area of the Al contact pad, $0.01 cm^2$, these values are assumed constant for each device. From the resistivity the conductivity of each device can be calculated via:

$$\sigma = \frac{1}{\rho}. \tag{2}$$

Data from the impedance spectra were analysed using the EIS Spectrum Analyser software package, with the |Z| converted to Z_{real} and $Z_{imaginary}$ components and frequency used. From this data an equivalent circuit can be plotted which can be used to show the nature of conduction through the device.

3.1 Control (BGW1)

To understand the effect that the Li_2S has had on the devices, first the results from the control device BGW1 will be discussed. Figure 3.1.1 shows a plot of current vs voltage for pad I8 of BGW1, assuming the device to be Ohmic in nature, represented by the dashed line, the resistance of the device is 3.76544×10^9 Ω in the 0.5V range is and 3.757849×10^9 Ω for the 1V range, from these values an estimate for the resistivity of the device can be calculated using (1) the resistivity of BGW1 was 3.76×10^{12} Ω cm. Then using (2), the conductivity of BGW1 is found to be 2.66×10^{-13} $(\Omega\ cm)^{-1}$, the conductivity of the control is therefore of the order 10^{-13} $(\Omega\ cm)^{-1}$. As literature currently available uses units of S cm^{-1} and these units are equivalent this report with henceforth use S cm^{-1} for consistency.

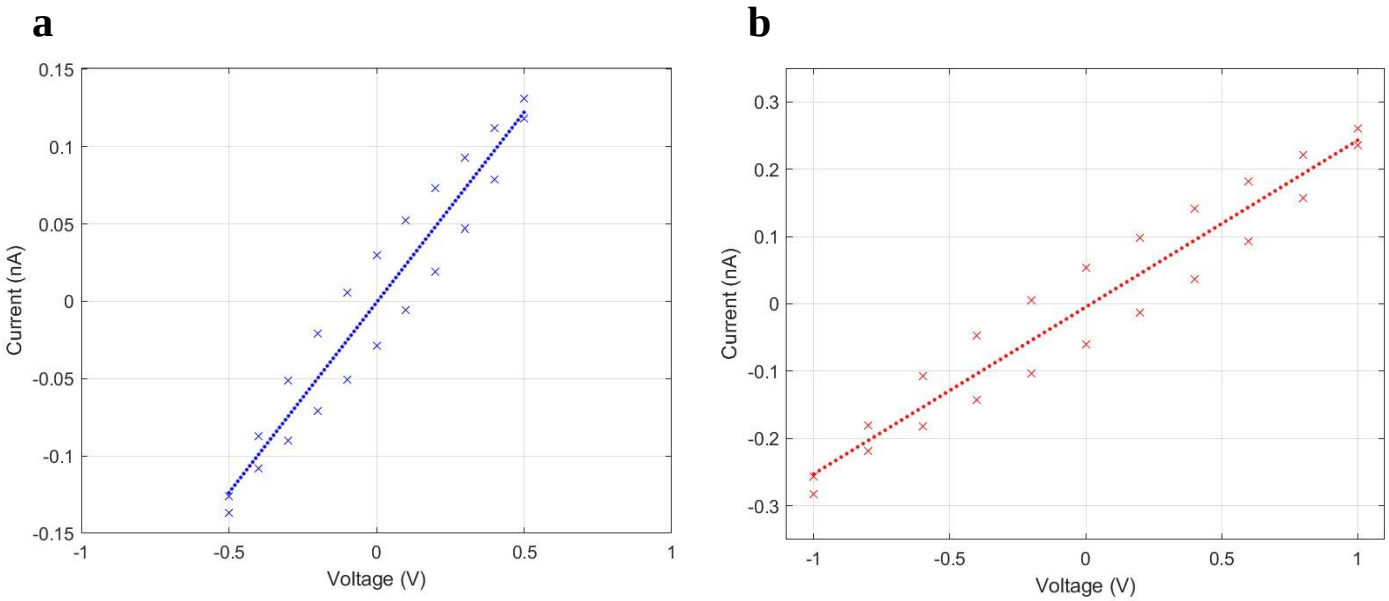

Figure 3.1.1.(a,b): Current vs Voltage for pad I8 of BGW1 in range ±0.5V (left) and in range ±1V (right).

An I-V sweep was also taken of pad J8 to test reproducibility of these values across the device, this data can be seen in figure 3.1.2.

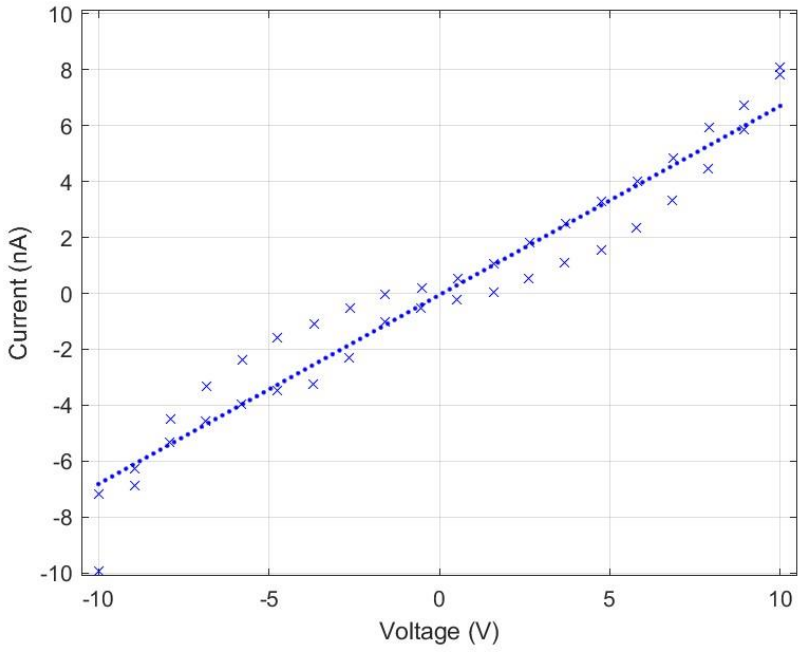

Figure 3.1.2: Current vs Voltage for pad J8 of BGW1 in range ±10V.

From this data, the resistance across the device is $1.3962 \times 10^{12}\ \Omega$ then using (1) and (2), the resistivity is found to be $1.3962 \times 10^{12}\ \Omega$ cm and the conductivity to be 7.16206×10^{-13} S cm^{-1}. As both values are of the same order of magnitude as their respective values found for pad I8 it can be

assumed that a resistivity of the order 10^{12} Ω cm and conductivity of 10^{-13} S cm^{-1} is characteristic of the whole device.

3.2 LN1

The first test device, denoted LN1, was fabricated with Li_2S deposited at a rate of 0.05 Å s^{-1} while GaLaS evaporation was at approximately 0.65 Å s^{-1}, this is taken as a rough approximation as exact data of the deposition rates was improperly recorded. Based on these values the ratio of GaLaS to Li_2S is estimated to be 13:1. Initial data from LN1 proved to show unusual behaviour with a clear discontinuity at -0.3V and 0.3V as can be seen in figure 3.2.1. In this test the voltage was swept from 0.5V to -0.5V.

To test whether this is characteristic behaviour of the device of an error within the setup of the apparatus of the experiment, the probes were reset onto pad H7 and in contact of the ITO and multiple sweeps were run both “up” and “down”, with the voltage range again being between -0.5V and 0.5V.

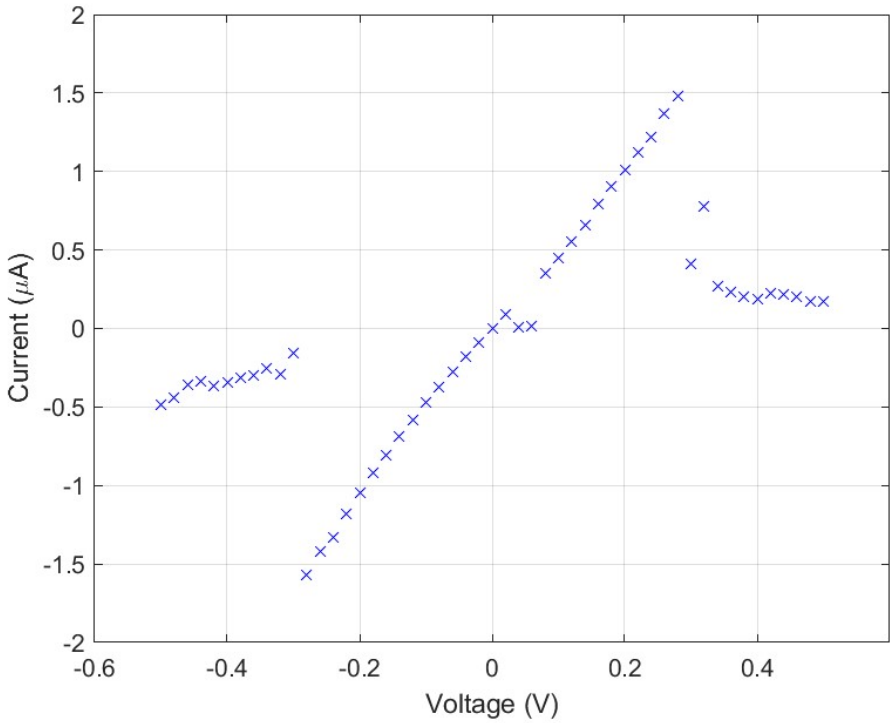

Figure 3.2.1: Current vs Voltage for LN1 in the range -0.5 to 0.5V.

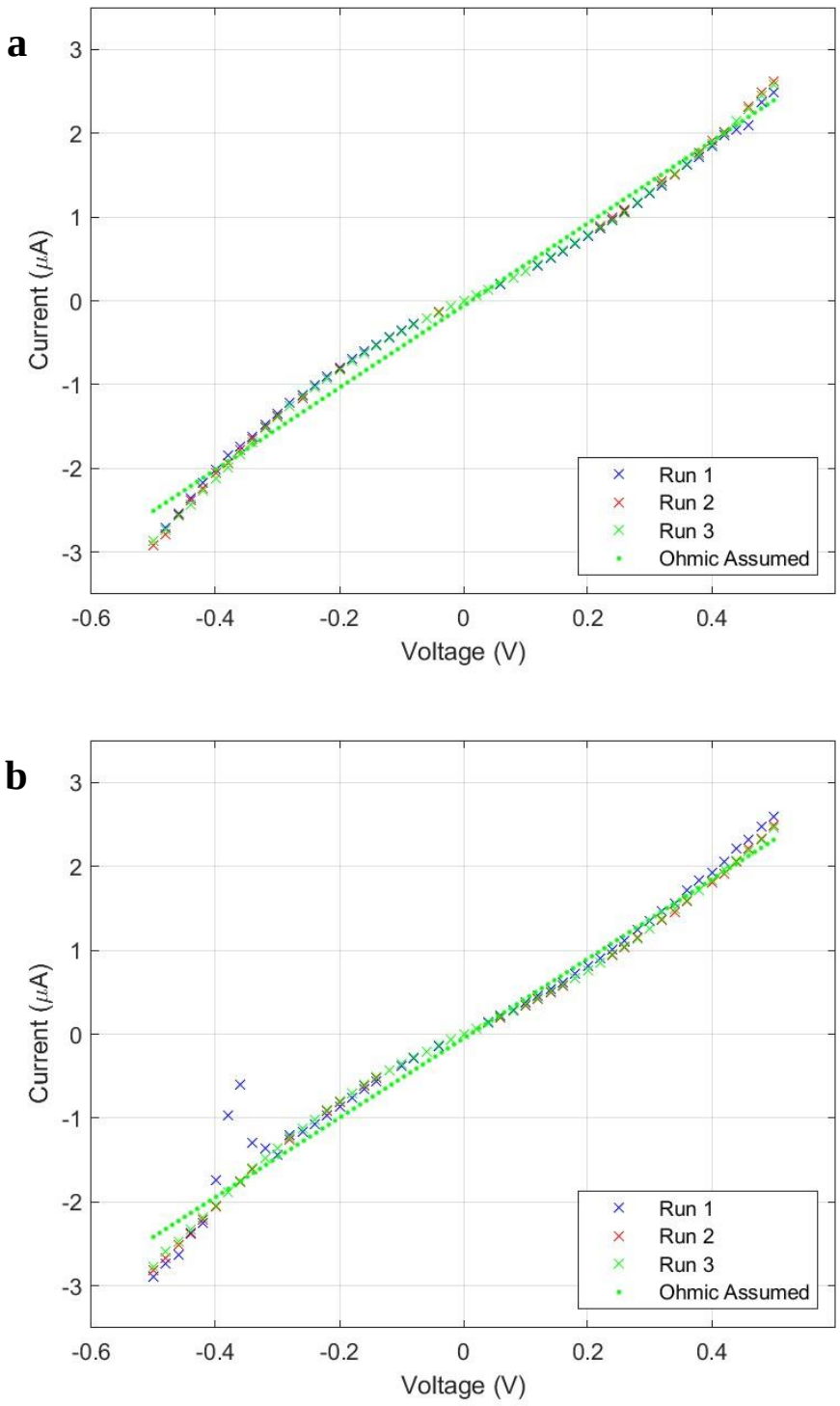

Figure 3.2.2.(a,b): Current vs Voltage for pad H7 in the range ± 0.5V, sweeps down (top), sweeps up (bottom).

Figure 3.2.2 clearly shows that, despite a small peak at -0.36V in run 1 of the up sweep, the data results from figure 3.2.1 were not reproducible and the subsequent data for figure 3.2.2 was reproducible, based on these new data points it is assumed that the data in figure 3.2.1 was due to improper set up of the experimental apparatus.

From figure 3.2.2.a and again approximating to Ohmic behaviour with resistance being calculated as 2.01922×10^5 Ω, using equation (1) the resistivity from the down sweeps is 2.01922×10^8 Ω cm, then using (2) the conductivity was 4.952399×10^{-9} S cm. From figure 3.2.2.b, the up sweeps, the resistance is 2.09370×10^5 Ω, the resistivity therefore, is 2.09370×10^8 Ω cm, giving a conductivity of 4.77622×10^{-9} S cm^{-1}, showing a conductivity on the order of 10^{-9} S cm for device LN1, comparing this value to the control's conductivity of 10^{-13} S cm^{-1}, demonstrates an increase in conductivity of 4 orders of magnitude despite having a GaLaS to Li_2S ratio of just 13:1, these initial results demonstrate the huge difference even just a small amount of Li_2S makes within the conduction layer.

Following the I-V testing, impedance spectra were taken of LN1.

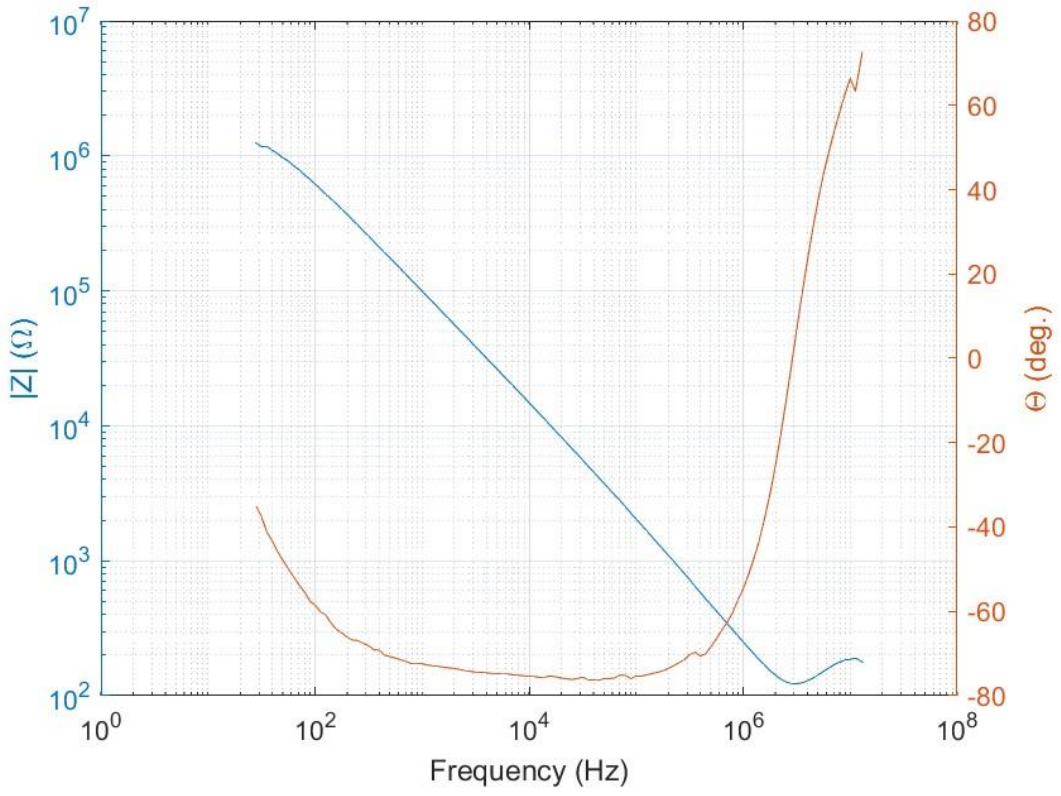

Figure 3.2.3: Impedance spectra of LN1.

This data was then passed to the EIS Spectrum analyser, with a Bode plot made and an equivalent circuit plotted.

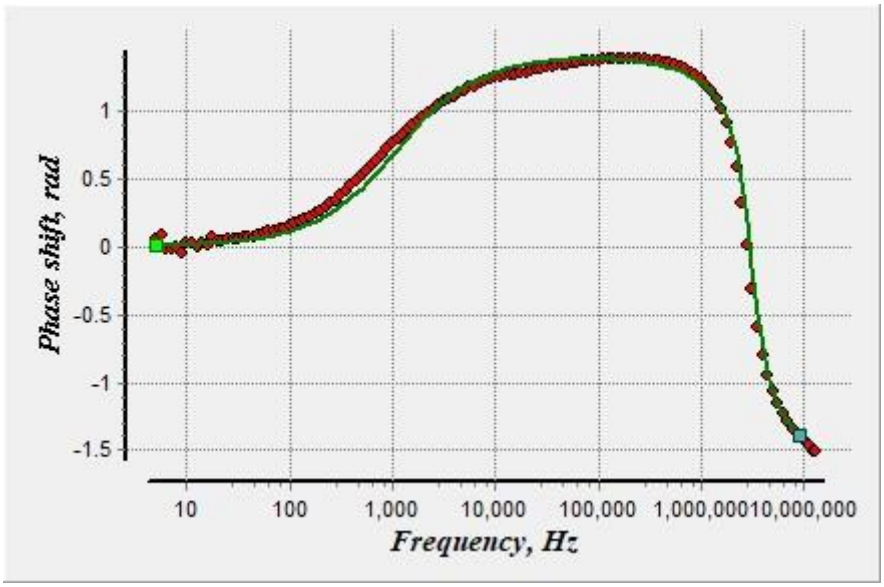

Figure 3.2.4: Bode plot of LN1 using pad H7, experimental data - red markers, simulated fit - green line.

The equivalent circuit used to create the simulated fit was as follows:

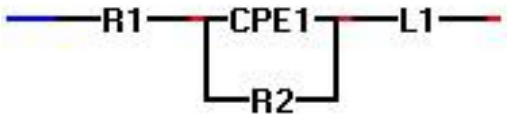

Figure 3.2.5: Equivalent circuit used in the impedance simulation. R1 = resistor 1, R2 = resistor 2, CPE1 = constant phase element 1, L1 = inductor 1.

The values of each circuit component were as follows:

Element	Value	Error (%)
R1 (resistor 1)	41.392 Ω	8.9506
R2 (resistor 2)	1.1168×10^5 Ω	2.7546
Q (Constant Phase Element, CPE1 constant)	3.1413×10^{-9}	7.0925
n (exponential factor of CPE1)	0.90108	0.48698
L1	4.6379×10^{-6} H	4.2088

Table 3.2.6: Values of each equivalent circuit component for LN1.

The CPE impedance is defined via:

$$\frac{1}{Z_{CPE}} = Q \cdot (i\omega)^n, \quad (3)$$

where Q is the CPE constant, i is the imaginary unit, ω is the frequency in Hz and n is the exponential CPE factor. The exponent can vary between 1 and 0, with n = 1 the impedance is that of an ideal capacitor, cases of n < 1 show non-ideal capacitive effects. A potential reason for the non-ideal effects can be caused by the jumping of ions within the sample, the jump of one ion to a neighbouring site causes other mobile ions nearby to rearrange or the original ion must jump back to its original position, these forward and backwards jumps cause non-ideal capacitive effects [9]. Therefore, with an n-value of 0.90108 it is assumed that the ion jumping is the cause in this case.

3.3 LN2

Based on the large increase in conductivity from a small amount of Li_2S in device LN1, for the next test device, LN2, a much larger amount of Li_2S was co-evaporated with the GaLaS, the powers for the evaporations and the total deposition rate can be seen in figure 3.3.1. At 45 W on the Li_2S crucible there was a deposition rate of 0.668 Å s^{-1} before the shutter was open. During the deposition the average power on the Li_2S boat was 52.5266 W, therefore, the rate of Li_2S deposition for the whole fabrication is assumed to be 0.668 Å s^{-1} as the powers were very close. For the GaLaS, the average power was 51.5144 W with an average deposition rate of 0.60655 Å s^{-1}. From these deposition rates the ratio of GaLaS:Li_2S was found as 0.908:1, from this the percentage of the conduction layer that is Li_2S was found to be 52.4%.

For this device three pads were tested each at 1V, data from pad H4 is shown in figure 3.3.2. From the Ohmic assumption the resistance is 171.2777 Ω. Using equation (1) the resistivity is found to be 1.71378×10^5 Ω cm, then using equation (2) the conductivity is 5.83506×10^{-6} S cm^{-1}.

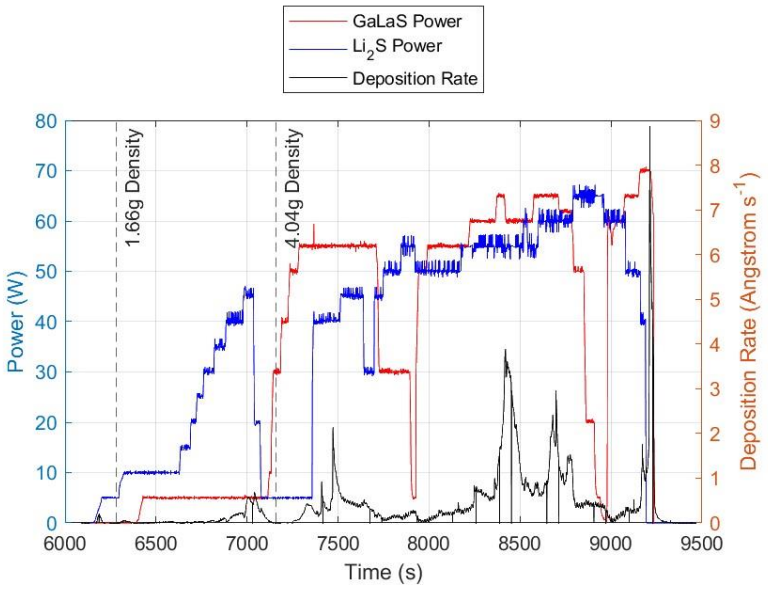

3.3.1: Plot of power vs time with deposition rate vs time. Dashed lines show at which point in time the density setting for the QCM is set to for the calculation of the deposition rate.

Figure 3.3.2 shows data from pad A6.

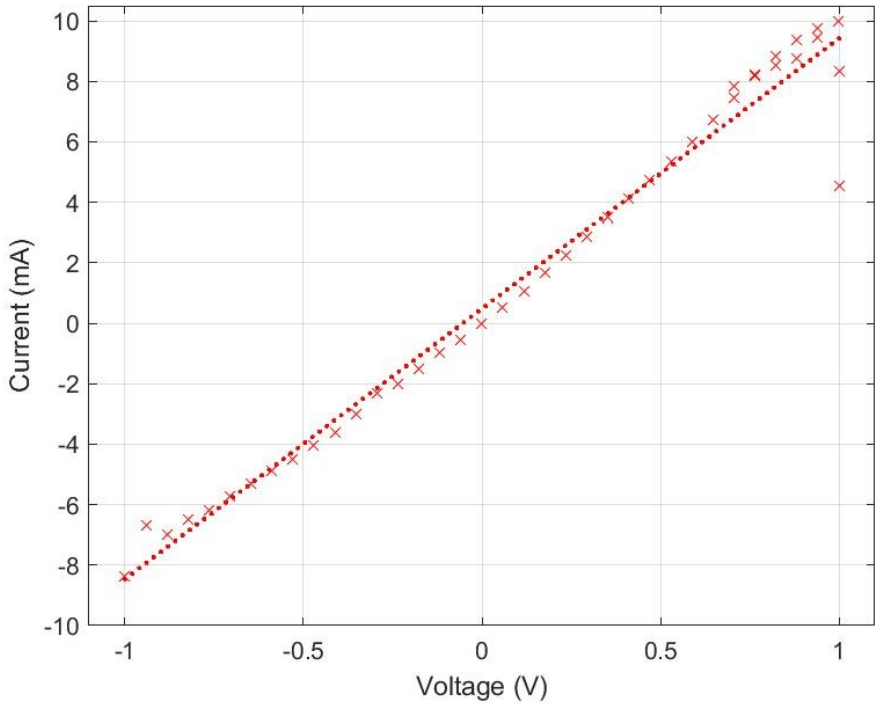

3.3.2: Voltage vs Current for pad A6 with Ohmic assumption represented by the dashed line.

From the Ohmic assumption the resistant on pad A6 is 108.90052 Ω. Using (1) the resistivity is found to be 1.08901×10^5 Ω cm then from (2) the conductivity is 9.18269×10^{-6} S cm^{-1}.

Data from pad D4 is shown in figure 3.3.4.

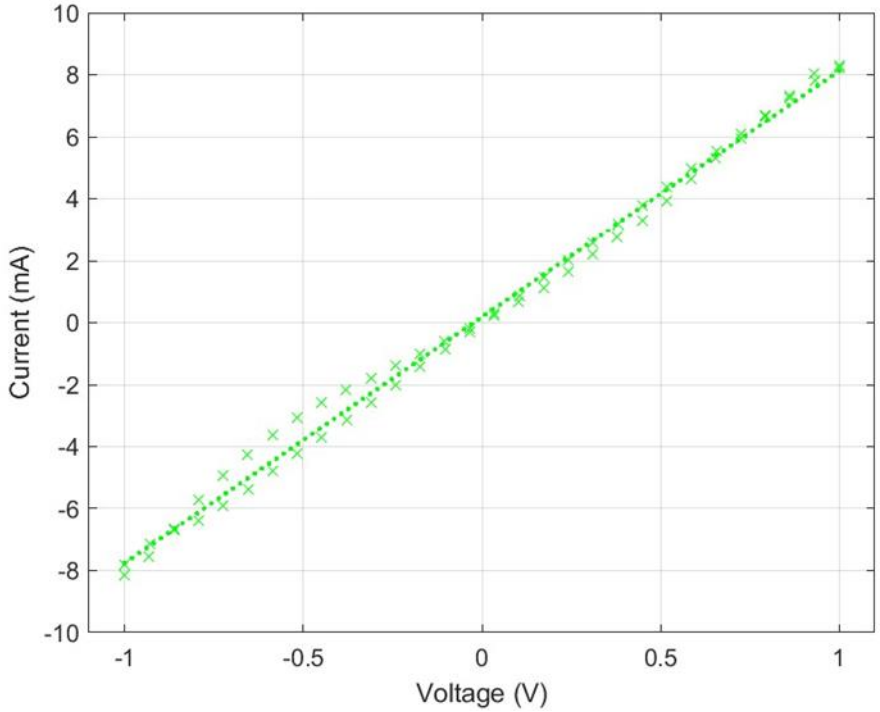

3.3.3: Voltage vs Current for pad D4, Ohmic behaviour assumption represented by the dashed line.

From the Ohmic assumption the resistance on pad D4 is 125.27524 Ω from (1) the resistivity is found to be 1.25275×10^5 Ω cm then from (2) the conductivity is found to be 7.98242×10^{-6} S cm^{-1}.

From these values a conductivity of the order of 10^{-6} S cm^{-1} is demonstrated for this device.

While having a drastic increase in conductivity when compared to LN1, the physical appearance of LN2 appeared different to both BGW1 and LN1 as these two devices are translucent in nature whereas LN2 appeared much opaquer. Due to this appearance, BGW1 and LN2 were imaged for closer inspection. Additionally, absorption spectra for all devices were taken at the end of the investigation. The analysis of this data can be found in section 3.5.

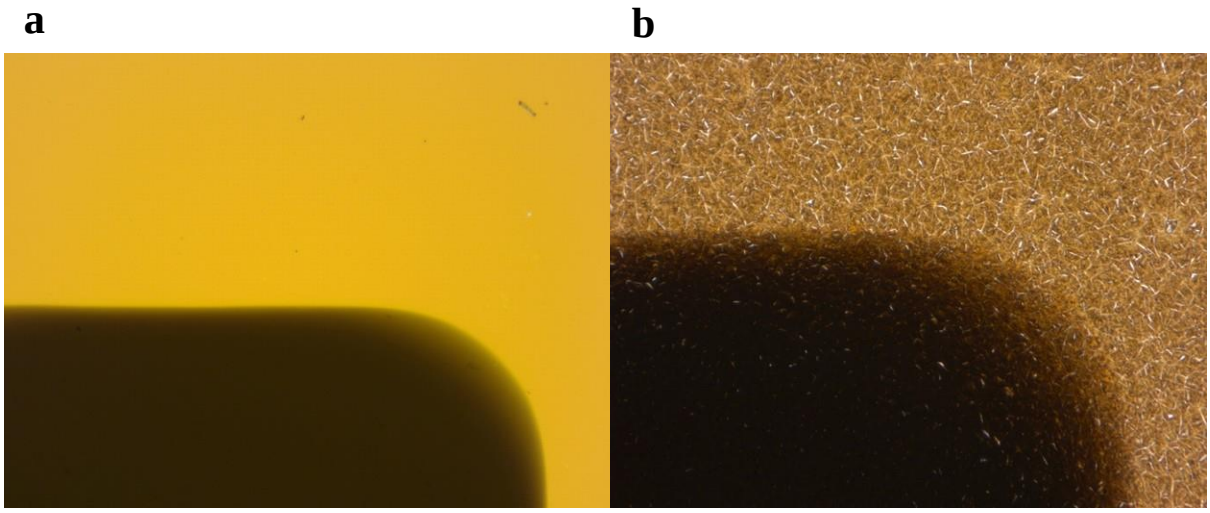

3.3.5.(a,b): Microscope images of BGW1 (left) and LN2 (right). Darker area in both images is an Al contact pad while the orange area is the conduction layer.

It can be clearly seen from figure 3.3.5 that in LN2 there is a much greater number of apparent cracks within the conduction layer, while this appears to have not directly affected the nature of the device's electrical characteristics, i.e. the nature of the I-V graphs still appears near ohmic in nature as with LN1, there is a potential that it may have affected the mechanical properties of the glass that are favourable for this materials usages such as potentially lowering its Young's modulus or affecting its transition temperature due to the lack of homogeneity throughout the conduction layer, however, in the scope of this investigation these properties were not tested.

It may be possible to prevent this phase separation from occurring (or more rather after fabrication treat the material to bring it back to a homogeneous phase) via heat treating. Previous studies of annealing the glasses to create glass ceramics composed of chalcogenide glasses that demonstrate high conductivities have been composed [10], therefore, further research into annealing GaLaS as an SSE could be promising.

Figure 3.3.6 - 7 show impedance spectra of LN2.

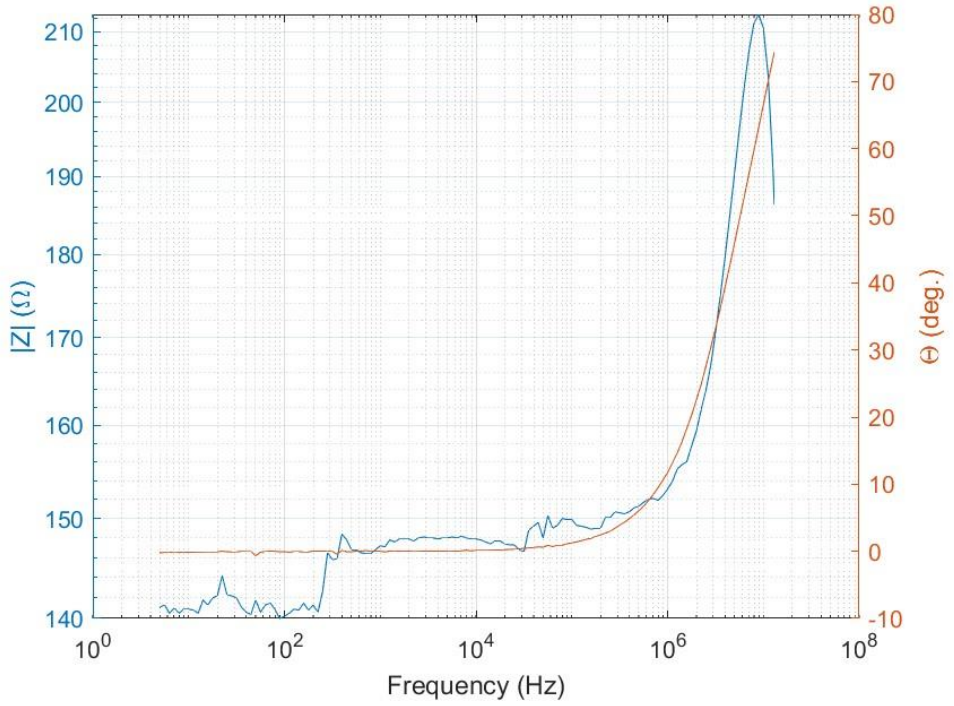

Figure 3.3.6: Impedance spectrum of pad A6.

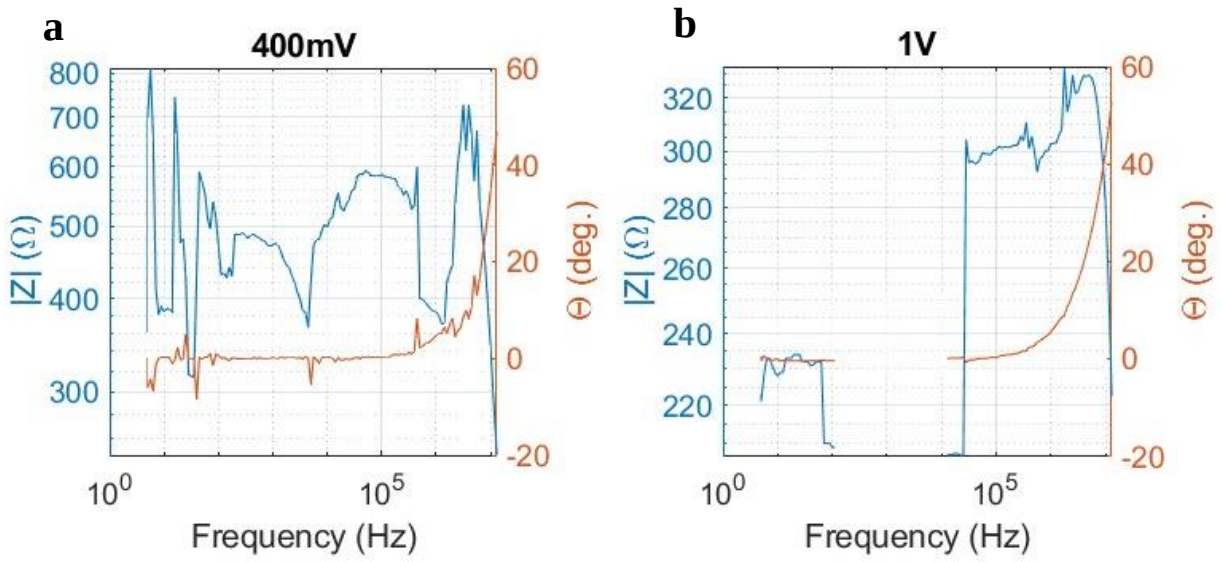

Figure 3.3.7.(a,b): Impedance spectra of pad H4 with the amplitude of the oscillation at 400mV(left) and 1V (right).

There clearly strange behaviour occurring within the device despite the near Ohmic nature seen in figure 3.3.2 and 3.3.3, this is likely due to the phase separation clear in the conduction layer.

As the data for pad A6 is the “cleanest” it is the data that is used in the circuit fitting.

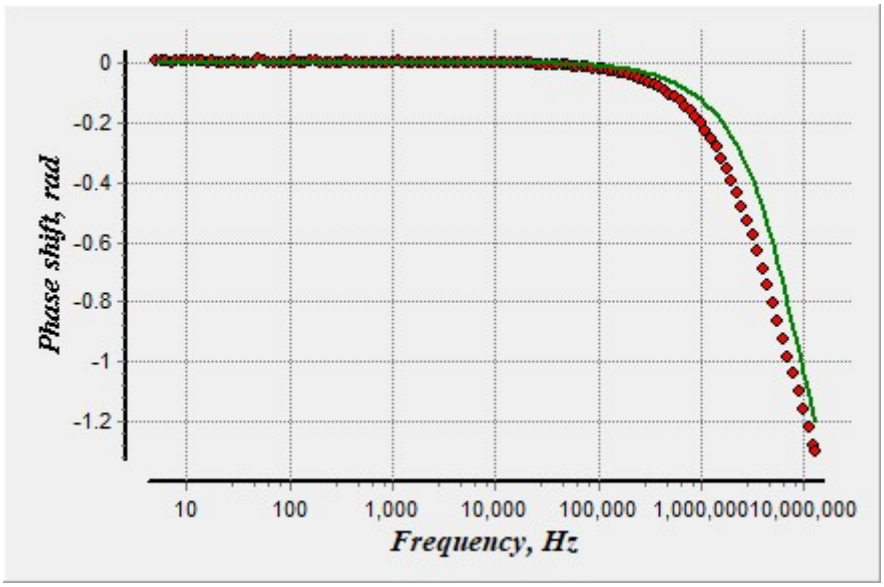

Figure 3.3.8: Bode plot for pad A6, experimental data - red dots, fitted plot - green line.

The fitted plot was obtained using the same circuit as used for LN1 as it was assumed that the equivalent circuits would be identical but with varying values for the parameters of each circuit element. The values for each circuit element were as follows:

Element	Value	Error (%)
R1 (resistor 1)	46.287 Ω	6.2243
R2 (resistor 2)	98.746 Ω	2.7546
Q (Constant Phase Element, CPE1 constant)	1.0153×10^{-10}	28.433
n (exponential factor of CPE1)	1	1.5604
L1	3.8833×10^{-6} H	4.2088

Table 3.3.9: Values of each equivalent circuit component for LN2

As in this case n = 1 it implies that the device is acting as an ideal capacitor [9], this is an unexpected behaviour, as the movement of the ions results in non-ideal capacitive properties as was explained in the previous section. Again, this unusual behaviour is likely to the phase separation that is present in LN2.

3.4 LN3

Due to the phase separation that was apparent within device LN2, despite its demonstration of the increase in Li_2S has on the increase in conductivity of the device, for this next device a lower amount of Li_2S was used so that no separation of phases occurred.

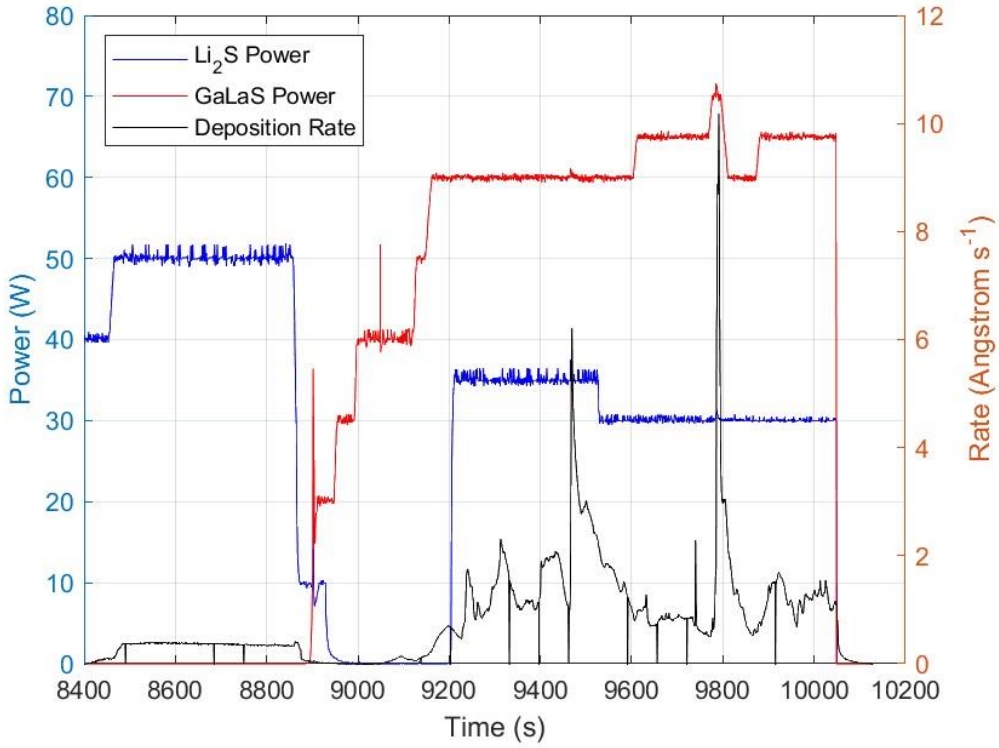

Figure 3.4.1: Power vs time with deposition rate vs time of the fabrication of LN3. Note initial power supplied to the Li_2S was conducted with the sample shutter closed to evaporate off any lithium hydroxide that may had potentially formed in the crucible.

As can be seen in figure 3.4.1 much lower powers of 35 W and 30 W were supplied to the Li_2S crucible compared to figure 3.3.1 for LN2, the appearance of the device appeared homogenous with no visible separation of states possibly due to the lower amount of Li_2S in this device the conduction layer. The total thickness of the conduction layer is known to be 1200 Å. It can be seen that when the Li_2S boat was at 50 W the average deposition rate was ~0.34 Å s^{-1}, as the average power during the deposition was 32.0106 W as this is 64.02% of the power, the average deposition rate is approximately 0.217 Å s^{-1}. As the average GaLaS deposition rate was 1.3651 Å s^{-1}, the ratio of GaLaS:Li_2S was approximately 6.29:1. From this ratio the Li_2S percentage in the conduction layer was approximately 13.717%.

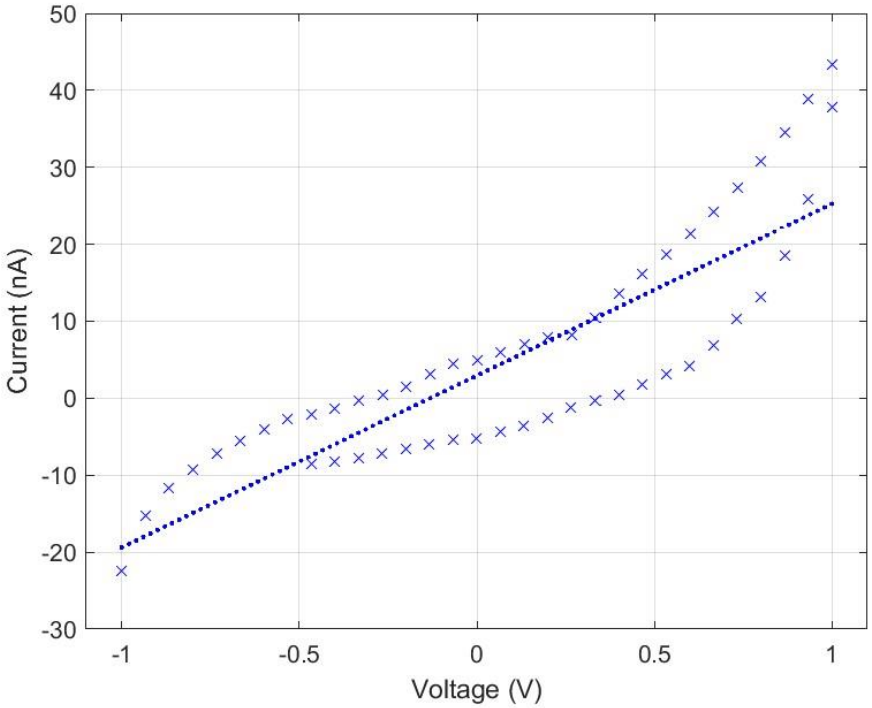

Figure 3.4.3: Current vs voltage for pad E6 of LN3, cyclic sweep in the ±1V range. Ohmic approximation represented by the dotted line.

As can be seen in figure 3.4.3, the nature of LN3 appears much more non-ohmic than previous devices in this investigation, therefore, the Ohmic approximation is not representative of the actual properties of this device. If, however, Ohmic approximation is assumed to be representative, from figure 3.4.3, the resistance is found to be 3.2847×10^{7} Ω, then using equation (1) the resistivity is found to be 3.1847×10^{10} Ω cm, then using (2) the conductivity is 3.04442×10^{-11} S cm^{-1} which is a very low value, 2 orders of magnitude lower than that of LN1 despite there being a comparable level of Li_2S content.

Due to the strange behaviour of this first set of results, more tests were run on the same pad at increasing voltage ranges. Figure 3.4.4 shows sweeps down in the 5V range, again strong non-ohmic behaviour exhibited by this device, however, there is a clear trend from subsequent sweeps of less current being conducted through the device at the same voltage ranges. As the final runs for both the up and down sweeps in figure 3.4.4 display a more Ohmic relation, an Ohmic approximation of these final datasets was assumed, shown in figure 3.4.5, note however, that the Ohmic approximation even for these datasets is clearly not representative of the true nature of the device.

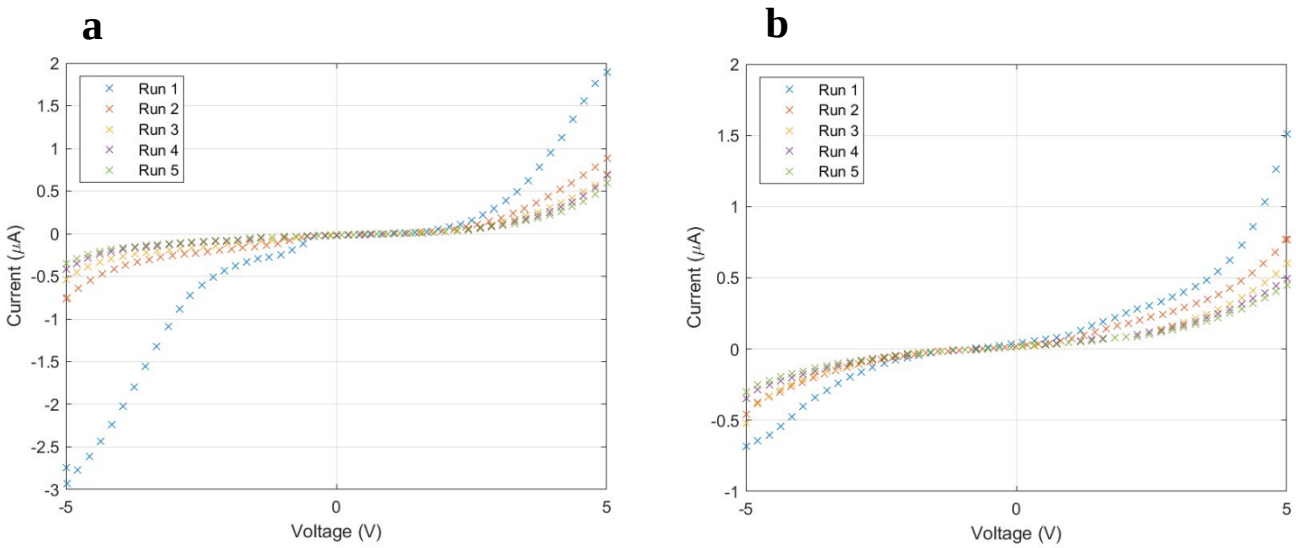

Figure 3.4.4.(a,b): 5V sweeps down (left) and up (down) showing clear trending towards higher resistance through the devices.

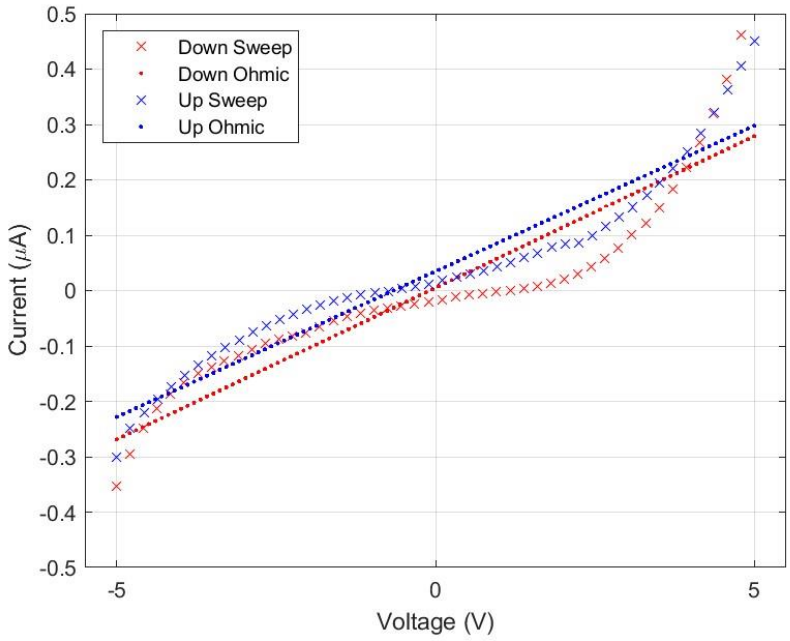

Figure 3.4.5: Final up and down 5V sweeps from figure 3.4.4 with Ohmic assumption also plotted.

From figure 3.4.5 for the down sweep the resistance was found to be $1.4885 \times 10^7 \Omega$, using (1) the resistivity was $1.4885 \times 10^{10}\ \Omega$ cm, then using (2) the conductivity was 6.7181×10^{-11} S cm^{-1}, following the same for the up sweeps, the resistance was $1.7371 \times 10^7\ \Omega$, the resistivity was $1.7371 \times 10^{10}\ \Omega$ cm and the conductivity was 5.7657×10^{-11} S cm^{-1}, again demonstrating a conductivity of 10^{-11} S cm^{-1} which is much lower than expected for the amount of Li_2S in the device.

To continue the investigation of the strange behaviour of this device, the range of voltage swept was increased up to 10V.

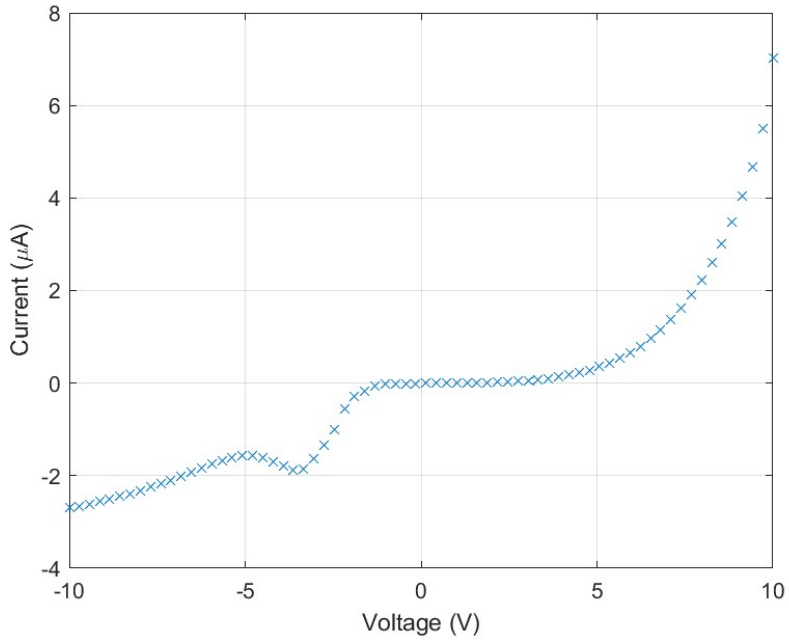

Figure 3.4.6: ±10V range sweep down for pad E6.

Figure 3.4.6 shows a 10V sweep across pad E6 showing very strange behaviour, of note is between -3V and -5V, as in this case the voltage was swept from positive to negative yet the current through the device became more positive. This test was repeated to test the reproducibility of this behaviour.

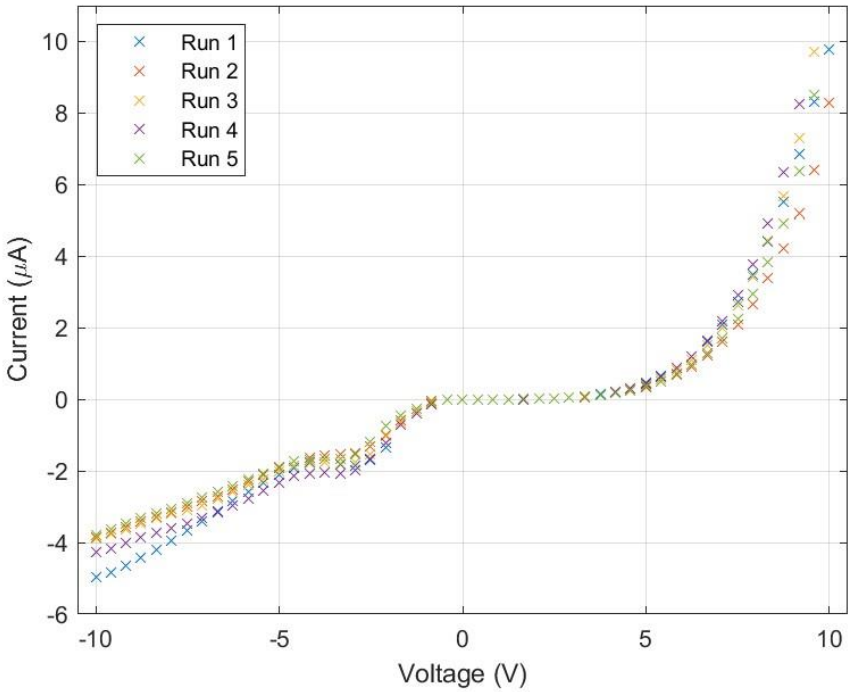

Figure 3.4.7: Multiple down sweeps of pad E6 in the ±10V range.

In figure 3.4.7 while the gradient at the inflexion around -3V is not as great as in figure 3.4.6, it is clear that the nature of this graph is characteristic of this device. During this testing the physical appearance of the Al contact pad also changed, shown in figure 3.4.8.

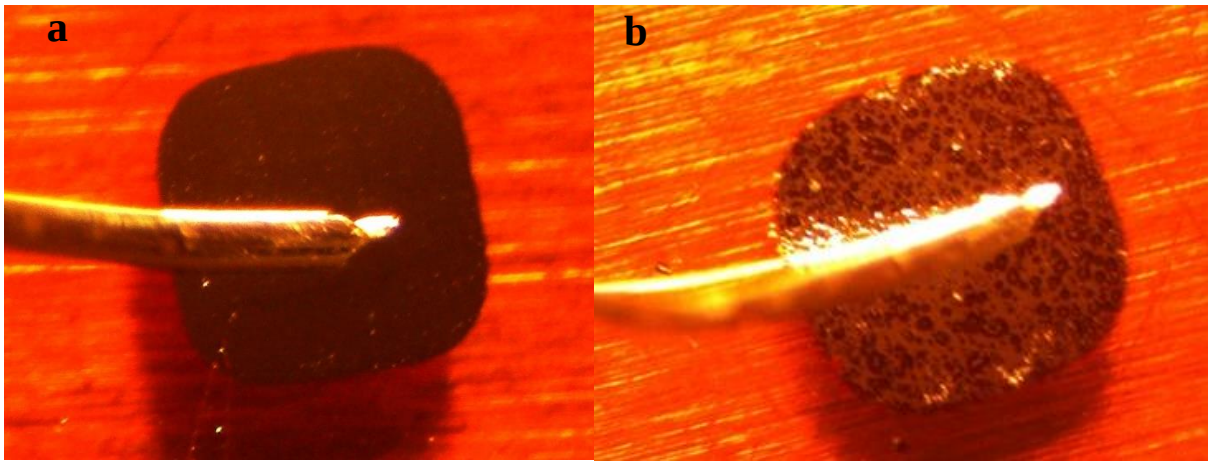

Figure 3.4.8.(a,b): Images of contact pad E6 prior to testing (left) and after testing (right).

It is believed that the appearance change seen was due to alloying between the Li in the condution layer and the Al that makes the contact pad, with this alloying being facilitated via the higher

voltages, the ability of Al and Li to alloy within Li containing electrolytes has been shown in previous studies [11].

Figure 3.4.9 shows the impedance spectra on pad E6 of LN3.

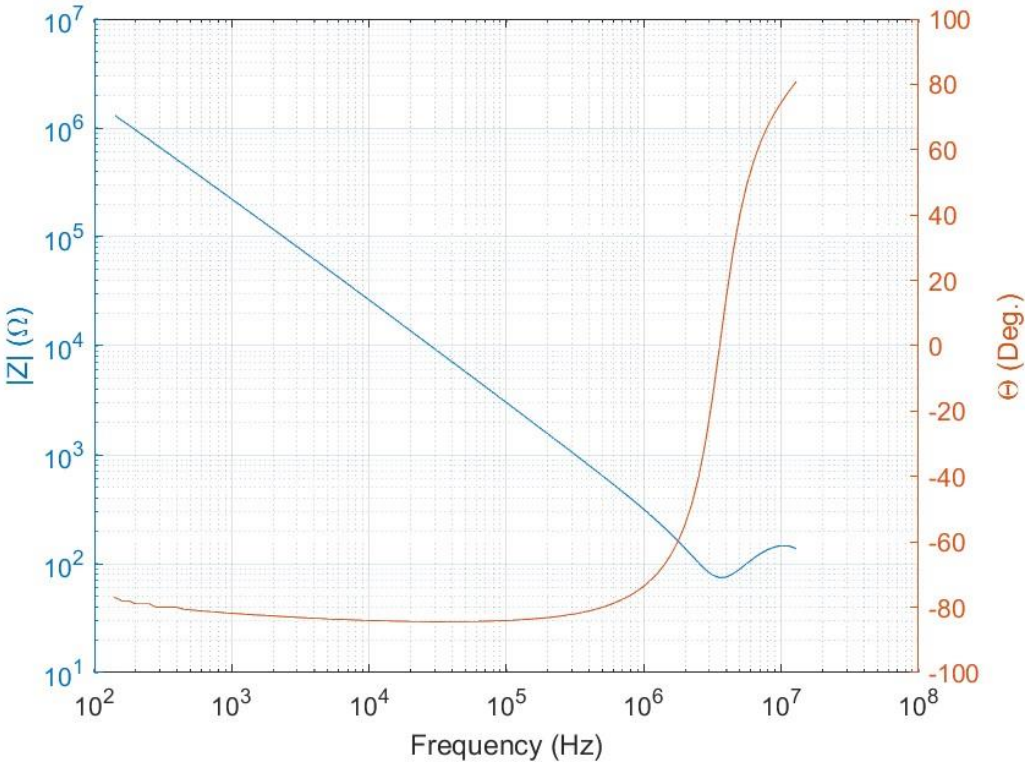

Figure 3.4.9: Impedance spectrum of pad E6.

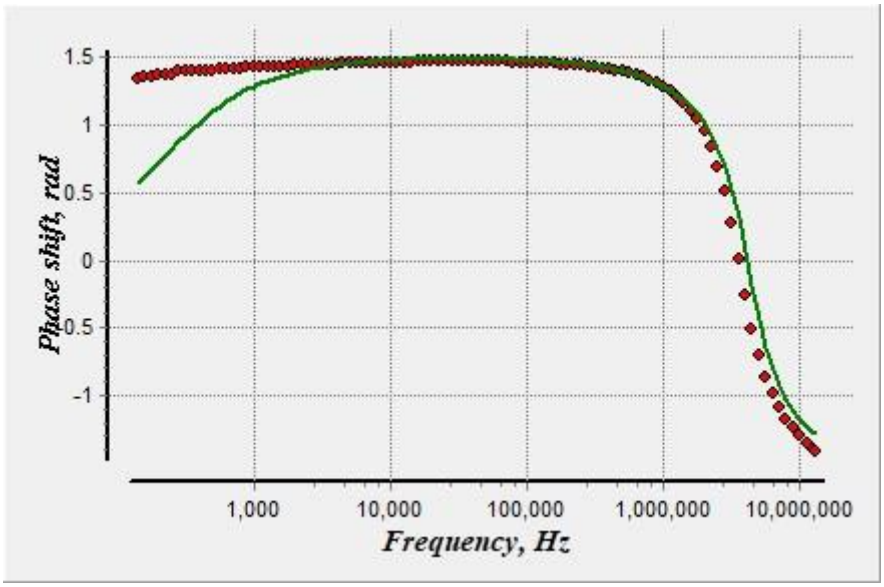

Figure 3.4.10: Bode plot with an amplitude of 1V on the oscillation. Experimental data – red dots, fitted plot – green line.

This plot was made using same equivalent circuit seen in figure 3.2.5. The fittment agrees very well with the experimental data for frequencies greater than ~2000 Hz, but has very poor agreement for <

2000 Hz. In these lower frequencies it is required for n > 1, demonstrating a physical limitation in the usage of a CPE in the equivalent circuit fitting [9].

Element	Value	Error (%)
R1 (resistor 1)	61.719 Ω	20.378
R2 (resistor 2)	1×10^{6} Ω	5.8106
Q (Constant Phase Element, CPE1 constant)	1.0007×10^{-9}	6.4545
n (exponential factor of CPE1)	0.95995	0.50575
L1	2.9702×10^{-6} H	11.851

Table 3.4.11: Values of all elements in the equivalent circuit plotted for LN3.

As n < 1 it is assumed that this shows ionic conduction as explained in section 3.2.

3.5 Absorption Spectra

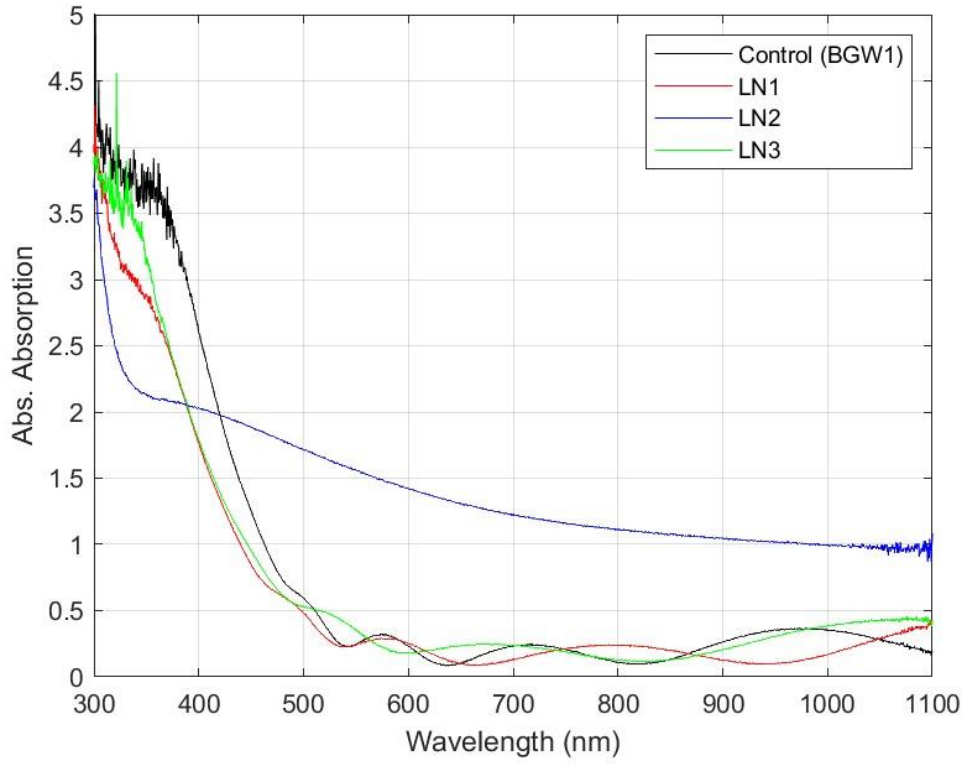

Figure 3.5.1: Absorption spectra of all devices.

From these spectra the band gap of the material can be approximated via finding the energy of the photons where there is a sudden increase in the absolute absorption of the material. This energy can be found via the photon energy:

$$E = \frac{hc}{\lambda \times 10^{-9}} \frac{1}{1.6 \times 10^{-19}}, \quad (4)$$

where E is the photon energy in eV; h is Planck's constant, 6.626×10^{-34} J s^{-1}; c is the speed of light 2.998×10^{8} m s^{-1} and λ is the wavelength of light in nm.

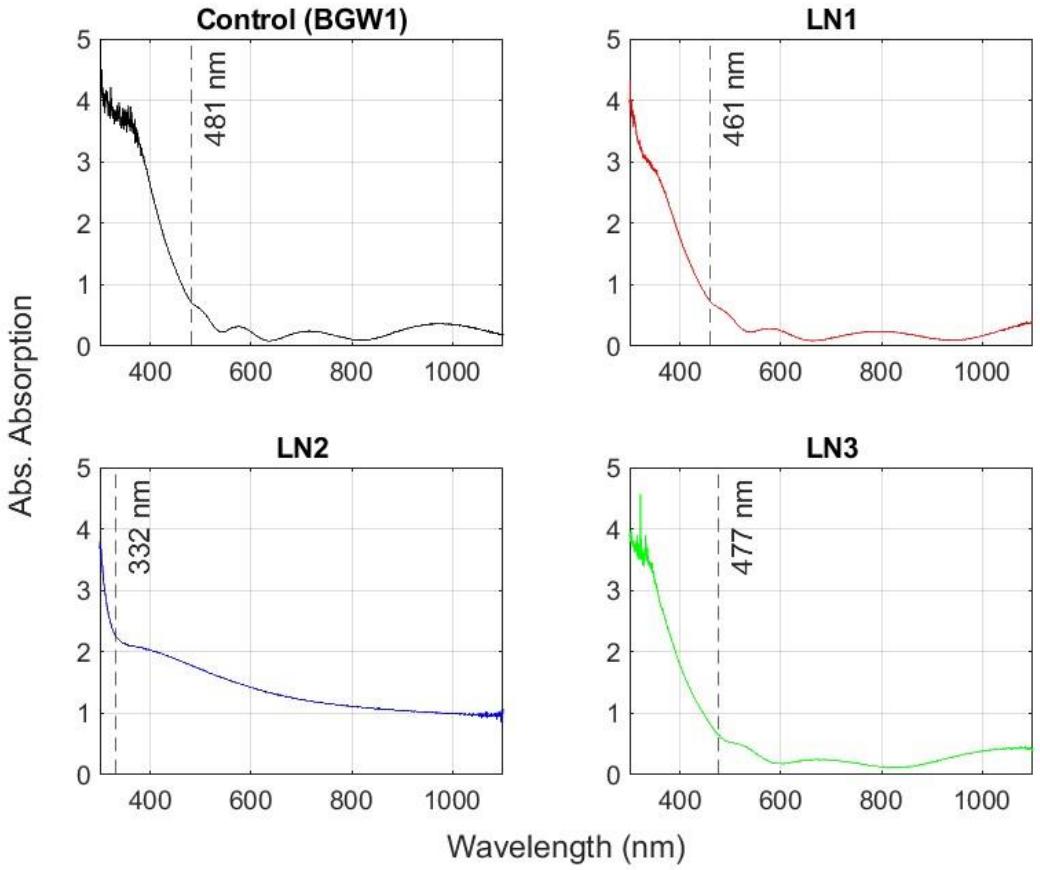

Figure 3.5.2: Absorption spectra of each device with the wavelength used to calculate the band gap indicated.

From these wavelengths the band gap energy for each device is as follows:

Device	Band Gap (eV)
Control (BGW1)	2.5812
LN1	2.6932
LN2	3.7396
LN3	2.6028

Table 3.5.1: Devices created within this investigation and their associated band gaps and Li content within the conduction layer.

The relatively broad band gaps present is likely too high to allow the transport of electrons at room temperature therefore, all conduction is likely via ionic conduction which is ideal for an electrolyte. It is known that only the electrons in the vicinity of the Fermi level can generate an electric field,

however, to calculate the Fermi level of the devices the density of states must be calculated which has not been covered within the scope of this investigation. Therefore, the assumption of no electron conduction due to the broad band gap has been assumed based on previous studies of other SSE's [12].

3.6 Final Results

Device Name	Conductivity (S cm^{-1})	Avg. Li_2S Power (W)	Li_2S (%)
BGW1 (Control)	10^{-13}	0	0
LN1	10^{-9}	10	0.0714 ± 10
LN2	10^{-6}	52.5266	52.4 ± 10
LN3	10^{-11}	32.0106	13.7 ± 10

Table 3.6.1: All devices fabricated within this investigation and their conductivities with associated Li_2S values.

Due to the QCM only being able to show the rate of deposition for one density and more in-depth determinations of the content of the devices such as an EDX scan have not been undertaken, an error in the calculation of the Li_2S content of 10% has been approximately chosen. Figure 3.6.2 shows each device's conductivity and its Li content.

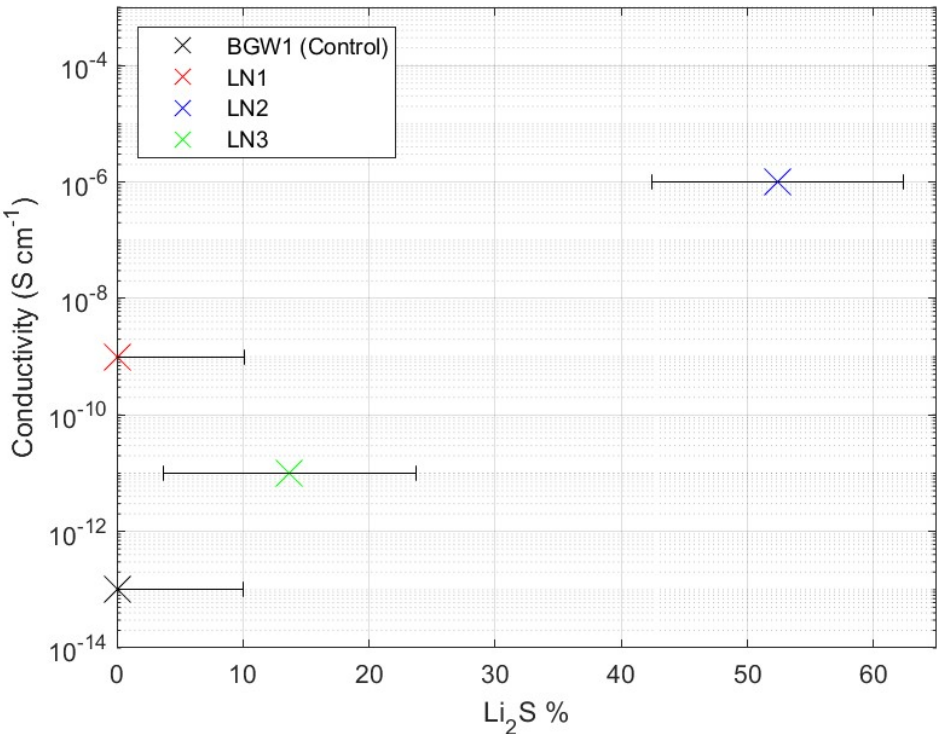

Figure 3.6.2: Conductivity vs Li_2S % for each device in this investigation.

4. Conclusion

In this paper the viability of gallium lanthanum sulfide as a solid-state electrolyte was investigated via means of thin film co-evaporation with lithium sulfide. The conductivity of the devices fabricated was calculated via data from voltage-current sweeps conducted on the devices and the conduction mechanism was discovered via analysis of the impedance of the devices. It was clearly demonstrated that great increases in conductivity of the devices can be achieved, with the absorption spectra and electrochemical impedance analysis implying that this conduction was indeed that of ionic conduction, there is indeed a potential for GaLaS to be used as an SSE. However, more investigation into the behaviour between the GaLaS and Li_2S at higher proportions of Li_2S (levels achieved for comparable SSEs have been as high as of the order of 80% Li_2S [13] which demonstrate conductivities comparable to that of current widespread liquid electrolytes) is needed. Additionally, at these higher temperatures methods to prevent the separation of phases present must be investigated and the effect that higher proportions of Li_2S has on the mechanical properties of GaLaS.

5. Bibliography

[1] Tollefson, J. (2022, February 28). *Climate change is hitting the planet faster than scientists originally thought*. Nature News. https://www.nature.com/articles/d41586-022-00585-7

[2] Tatsumisago, M., Mizuno, F., & Hayashi, A. (2006). All-solid-state lithium secondary batteries using sulfide-based glass–ceramic electrolytes. *Journal of Power Sources*, *159*(1), 193–199. https://doi.org/10.1016/j.jpowsour.2006.04.037

[3] Zhang, Q., Cao, D., Ma, Y., Natan, A., Aurora, P., & Zhu, H. (2019). Sulfide-based solid-state electrolytes: Synthesis, stability, and potential for all-solid-state batteries. *Advanced Materials*, *31*(44). https://doi.org/10.1002/adma.201901131

[4] Kamaya, N., Homma, K., Yamakawa, Y., Hirayama, M., Kanno, R., Yonemura, M., Kamiyama, T., Kato, Y., Hama, S., Kawamoto, K., & Mitsui, A. (2011, July 31). *A lithium superionic conductor*. Nature News. https://www.nature.com/articles/nmat3066

[5] Hughes, M. A., Burgess, A., Hinder, S., Gholizadeh, A. B., Craig, C., & Hewak, D. W. (2018). High speed chalcogenide glass electrochemical metallization cells with various active metals. *Nanotechnology*, *29*(31), 315202. https://doi.org/10.1088/1361-6528/aac483

[6] Sreeram, A. N., Varshneya, A. K., & Swiler, D. R. (1991). Molar volume and elastic properties of multicomponent chalcogenide glasses. *Journal of Non-Crystalline Solids*, *128*(3), 294–309. https://doi.org/10.1016/0022-3093(91)90467-k

[7] Soraya, M. M., Abdel-Wahab, F., Elamin, A. A., Shaaban, E. R., & Ali Karrar, N. N. (2023). Structural and thermal characteristics of GE30−XSBXTE10SE60 ($0 \leq x \leq 20$) glasses for electronic devices. *Journal of Thermal Analysis and Calorimetry*, *148*(13), 5927–5942. https://doi.org/10.1007/s10973-023-12165-6

[8] Aly, K. A., Abdel Rahim, F. M., & Dahshan, A. (2014). Thermal analysis and physical properties of bi–se–te chalcogenide glasses. *Journal of Alloys and Compounds*, *593*, 283–289. https://doi.org/10.1016/j.jallcom.2014.01.057

[9] Shoar Abouzari, M. R., Berkemeier, F., Schmitz, G., & Wilmer, D. (2009). On the physical interpretation of constant phase elements. *Solid State Ionics*, *180*(14–16), 922–927. https://doi.org/10.1016/j.ssi.2009.04.002

[10] Pradel, A. (2017). Chapter 21: Nucleation, crystallisation and phase separation in chalcogenide glasses. In *From glass to crystal: Nucleation, growth and phase separation: from research to applications* (pp. 483–484). essay, EDP Sciences.

[11] Yang, J., & Wang, J. (2009). Secondary batteries – lithium rechargeable systems – lithium-ion | negative electrodes: Lithium alloys. *Encyclopedia of Electrochemical Power Sources*, 225–236. https://doi.org/10.1016/b978-044452745-5.00190-8

[12] Dai, H., Xu, W., Hu, Z., Chen, Y., Gu, J., Xie, F., Wei, W., Guo, R., & Zhang, G. (2021). Novel solid-state sodium-ion battery with wide band gap Nati2(PO4)3 Nanocrystal electrolyte. *ACS Omega*, *6*(17), 11537–11544. https://doi.org/10.1021/acsomega.1c00664

[13] Tatsumisago, M., & Hayashi, A. (2014). Chalcogenide glasses as electrolytes for batteries. *Chalcogenide Glasses*, 632–654. https://doi.org/10.1533/9780857093561.2.632